International Journal of Chemical Science
www.chemicaljournals.com
Online ISSN: 2523-2843, Print ISSN: 2523-6075
Received: 10-07-2021, Accepted: 21-07-2021, Published: 13-08-2021
Volume 5, Issue 4, 2021, Page No. 29-38

Pt, N co-doped TiO_2 ternary nanocomposite associated with activated carbon for the photocatalytic degradation of Methylene blue: optimization and modeling using the taguchi design

Nkeng Severin Muluh[3*], Njoyim Estella Buleng Tamungang[1], Julius Numbonui Ghogomu[2], T D Noufame[3]

[1] Department of Chemistry, Higher Teacher Training College, University of Bamenda, Bambili, Cameroon

[2] Department of Chemistry, Faculty of Science, University of Bamenda, Bambili, Cameroon

[3] Department of Chemistry, Faculty of Science, University of Dschang, Dschang, Cameroon

Abstract

Two photocatalysts Pt, N co-doped TiO_2 (Pt-N-TiO_2) and Pt, N co-doped TiO_2 associated with Raphia Hooker epicarp activated carbon (Pt-N-TiO_2/RHEAC) were synthesized via the sol-gel method. The as-prepared photocatalysts were characterized for their surface areas via the BET method, pore size distribution via the BJH method, and bandgap energy using diffuse reflectance spectroscopy. Both photocatalysts exhibited mesoporous structures with cylindrical pore structures having mean pore diameters of 27.86nm and 37.09nm and bandgap energies of 3.05eV and 2.83eV for Pt-N-TiO_2 and Pt-N-TiO_2/RHEAC respectively. Taguchi design was employed for the optimization and modeling of the process parameters which were dye concentration, amount of catalyst, irradiation time, and pH. The photodegradation efficiencies of methylene blue removal by both catalysts were 77.58% and 83.38% for Pt-N-TiO_2 and Pt-N-TiO_2/RHEAC respectively under optimum conditions. Furthermore, the mathematical models developed exhibited high correlation coefficients (R^2) of 96.23% and 97.38% for the photodegradation efficiencies by Pt-N-TiO_2 and Pt-N-TiO_2/RHEAC respectively between the predicted and the experimental response characteristics. This was an indication that both models could be effectively utilized in predicting the response characteristics at the optimum process parameters level. The amount of catalyst and dye concentration were the only process parameters that contributed meaningfully to MB removal.

Keywords: orthogonal array, photocatalytic degradation, signal-to-noise ratio, statistical optimization, taguchi design, ternary nanocomposite

Introduction

The presence of dye molecules in the environment and water bodies is of major concern not just because of their toxicity but equally due to their threat to human life and the environment. Water contaminated with dye is not only unfit for drinking by both humans and animals however, due to its marked inhibitive actions on the photosynthetic process in water plants and phytoplankton, dye wastewater is not suitable for agricultural irrigation. In addition, dyes reduced the dissolved oxygen of the aquatic ecosystem leading to an increase in Chemical Oxygen Demand (COD) [1]. Hence, the sustainable removal of these unwanted contaminants from wastewater and their degradation has become a major challenge for scientists.

Methylene Blue (MB) is a heterocyclic aromatic compound (Table 1). It has a characteristic deep blue colour [2] Methylene blue has extensive applications. It is employed not only to dye paper but also to tint silk. Predominantly, Methylene blue has been applied in human and veterinary medicine for several diagnostic and healing procedures [3]. Methylene blue significantly causes pollution to the environment, it is arduous to degrade methylene blue using the conventional wastewater treatment methods which include biological treatment, coagulation, flotation, electrochemical techniques, adsorption, and oxidation, as a result of its immense stability against decomposition by heat, light and chemicals, its complex aromatic structure, and its hydrophilic nature [4].

In recent years, photocatalysis, an advanced oxidation process (AOP) has been utilized for the sequestration of methylene blue dye molecules from wastewater using nanoparticles semiconductors. A considerable number of photocatalysts have been suggested, developed, and used to remove methylene blue from industrial effluents. They include Pd-supported Cu-doped Ti-pillared montmorillonite catalyst [5], Modified TiO2/BiVO4 photocatalysts [6], Mn-doped ZrO2 nanoparticles [7], MgO-SCCA-Zn hybrid ozonation catalyst [8], Fe3O4/TiO2 core/shell nanocubes [9], magnetic SrFe12O19 [10], ZnO/NiFe2O4 nanoparticles [11], Co-Mn-Fe complex oxide catalysts [12], CdS nanowire [13], silver nanoparticle decorated polymeric spheres [14], and Au/ZnO-CeO2 [15].

Because of their stability, non-toxicity, low cost, and resistance to both chemical and optical corrosion, TiO2 based photocatalysts have been demonstrated to be the most efficient for a wide range of energy and environmental applications [16]. However, the inherent TiO2 bandgap energy of 3.2 eV implies photon excitation can only take place under UV light irradiation. Sunlight is made up of roughly 5% UV, 43% visible and 52% IR [17]. Therefore, the large bandgap of TiO2 restricts its photocatalytic activity using visible light, which in turn limits its usage in applications involving visible light. The swift recombination of the electron-hole pairs that are photogenerated is another limitation that greatly reduces the photodegradation efficiency of the photocatalyst under normal conditions [18]. These limitations can be improved upon by doping TiO2 with non-metal atoms such as N or noble metal

nanoparticles [19]. The non-metal atom provides the narrowing of the bandgap by shifting the absorption spectrum to the visible region [20] and the metal nanoparticles suppress the recombination of the electron-hole pair since the metal acts as an electron sink which can promote interfacial charge transfer and consequently less charge recombination [21]. Furthermore, it is a challenging task to recover pure TiO2 powder from the treated wastewater, thereby limiting the practical applicability of TiO2. Thus far, the problem has been tackled by immobilizing the photocatalyst using a variety of porous materials as support [22]. Several porous materials such as zeolites, glass, and activated carbon, etc., have been examined [23, 24, 44]. Amongst these porous materials, activated carbon has been widely employed as photocatalyst support because they have large specific surface areas and rich functional groups [26, 27]. Furthermore, photocatalysts synthesized with activated carbon as substructure can adsorb a large proportion of noxious substances formed during the photodegradation process. Thus, integrating the photocatalytic activities of the photocatalyst with the adsorptive properties of the activated carbons generates a cooperative effect leading to the improvement of the efficiency of the photocatalysts [28]. Statistical optimization using multivariate methods has several benefits in comparison to traditional methods such as the one-factor-at-a-time (OFAT) since they can assist in obtaining more data with fewer experimental runs [29]. The fundamental principles of the Taguchi approach are to acquire information about the main effects and interactive effects of the process parameters from the lowest number of experiments [30].

In this work, all of the process parameters were optimized by employing the Taguchi design to realize the optimal photodegradation of methylene blue dye from an aqueous solution. This procedure has been utilized in the literature by several other researchers for the optimization of the experimental process parameter using AOP [31, 32]. To our understanding, literature on process optimization and modeling of photocatalytic degradation of methylene blue using the Taguchi design is somewhat scarce. There is no study in literature dedicated to Taguchi design optimization of photocatalytic degradation of methylene blue using Pt, N co-doped TiO2 ternary nanocomposite with raphia hookeri epicarp activated carbon (RHEAC) serving as a support matrix. Thus, it is worth studying exhaustively the influence of activated carbons as a framework to support Pt-N-TiO2 photocatalyst in the photocatalytic degradation of methylene blue and the statistical optimization and modeling of the process using Taguchi design. Minitab software version 17 was used for the design of experiments, analysis of results, optimization, and modeling of the process.

Table 1: Chemical structure and characteristics of methylene blue dye

Name	Molecular Structure	Chemical Structure	Molar Mass (gmol-1)	λmax (nm)
Methylene Blue	C16H18ClN3S	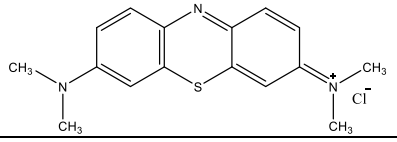	319.85	664

Material and Method

Materials and instrumentation

All chemicals utilized were of analytical reagent grade quality and used without further purification. All solutions were prepared with double-distilled water.

- Methylene blue, sodium hydroxide, hydrochloric acid were all Merck products, TiCl4 and urea were from BDH company, absolute ethanol (Prolabo). The chemicals were all supplied by LabSec.
- The surface area and other surface properties of the catalysts were assessed by an ASAP-2000 (Micromeritics, USA) nitrogen gas adsorption analyzer at 77K.
- UV-Vis spectra for bandgap energy studies were performed using a DRS Lambda 35 (Perkin-Elmer, USA) with BaSO4 used as the reference substance.
- Residual MB concentration in the filtrate and UV-Vis absorption spectra during photodegradation studies were obtained using a UV-Vis spectrophotometer (JENWAY).

Preparation of the photocatalyst

To prepare Pt, N co-doped TiO2 photocatalyst, a standard sol-gel approach was utilized [16]. First, 5 mL TiCl4 was added to 10 mL of 1M HCl acid solution in a beaker while vigorously stirring in an ice/water mixture. 2 g of urea and 15 ml aqueous solution of chloroplatinic acid (H2PtCl6.6H2O, 5 wt %) was added to the reaction mixture. The combination was stirred at 105°C for 5h. After cooling to room temperature, the colloidal suspension was filtered and the solid obtained was washed several times with distilled water and the wash water was tested with 0.1M AgNO3 solution to ensure no Cl- ions were detected. After the washing, the Cl- ions free solid was dried in the oven at 70°C overnight. The resulting powder was then calcined at 450°C for 5h under air.

To prepare the Pt-N-TiO2/RHEAC photocatalysts, first, 2 g of raphia hookeri epicarp activated carbon (RHEAC) was digested in 200 mL ethanol for 1h under sonication and 0.2 g of the as-prepared Pt-N-TiO2 photocatalyst was also dissolved in 50 mL ethanol for 30 min. both solutions were then blended and the mixture was sonicated for 1h and then stirred at 300 rpm for 24h. The resulting sample was then separated by centrifugation and dried at 80°C for 4h. The dried sample is denoted Pt-N-TiO2/RHEAC.

Experimental design based on the Taguchi approach

The Taguchi Orthogonal Array (OA) method is a Design of Experiments (DOE) technique that is frequently utilized to obtain information about the optimal performance of a process. In the OA experimental design, the columns for the independent variables are orthogonal to one another [29]. The primary objective of the Taguchi method is to determine the best combination of process parameters that reduce the variability in the response. The approach consists of (i) the design of the experiment, (ii) carrying out the experiment, and (iii) analysis of results. The experimental results obtained following the Taguchi OA approach are examined

to accomplished one or more of the following three goals [33]:

1. To find out the trend of influence of factors and interactions under investigation;
2. To identify the significant factors and their relative impact on the variation of results;
3. To establish the optimum conditions for the process, along with:

A. an approximation of the individual factor's contribution,
B. a forecast of anticipated response under the optimum conditions.

In this study, the Taguchi L9 OA experimental design consisting of four process parameters each having three levels was utilized as presented in Table 2. The signal-to-noise ratio (S/N) and analysis of variance (ANOVA) were used to analyze the results of designed experiments.

S/N ratio in Taguchi design is defined as the ratio between desirable results (signal) to undesirable results (noise) and the maximum S/N ratio gives the optimum conditions [29]. The following three functions: larger-the-better, smaller-the-better, and nominal-the-best are usually used in describing the S/N ratio. In this study, the objective was to achieve maximum photodegradation efficiency of MB dye, so the larger-the-better S/N ratio was utilized.

$$\frac{S}{N} = -10\log\left[\frac{1}{n}\sum_{i=1}^{n}\frac{1}{y_i^2}\right] \quad (1)$$

Where *yi* is the characteristic property, n is the replication number of the experiment.

Table 2: Process parameters and their levels

Process Parameter	Units	Symbol	Level		
			1	2	3
Dye Concentration	ppm	*C*	15	25	35
Amount of Catalyst	g	*A*	0.3	0.6	0.9
Irradiation Time	min.	*T*	60	90	120
pH		*P*	5.5	7	8.5

Photocatalytic Degradation Process

The photocatalytic degradation of methylene blue dye using the as-prepared photocatalysts was accomplished per the L9 OA experimental plan presented in Table 3. The experiments were performed randomly to minimize systematic error. First, the photocatalysts were added to 25 mL of dye solution in a 100 mL beaker. The pH of the dye solution containing the photocatalyst was then adjusted to the desired pH value using either 0.1M NaOH or 0.1M HCl solution. The mixture in the beaker was then stirred using a magnetic stirrer at 250 rpm. The beaker and its content were then subjected to irradiation axially using a 1000 W halogen xenon lamp for a fixed time interval. The photodegradation experiment was performed at room temperature. To determine the remaining methylene blue concentration, 5 mL aliquots were withdrawn from the sample at appropriate time intervals and filtered to separate solid catalyst particles. The filtrate was taken into a cuvette and the concentration was measured using a UV-Visible Spectrophotometer which measured the absorbance at 664 nm, wavelength at which the absorption of methylene blue is maximal. A calibration curve based on Beer-lambert's law was established by linking the absorbance to the concentration. The photodegradation of methylene blue described in terms of percentage photodegradation efficiency (% η) was calculated using equation (2) [34].

$$\%\,\text{Photodegradation}(\eta) = \left(1 - \frac{C_f}{C_0}\right) \text{x}\, 100 \quad (2)$$

Where η1 and η2 are the percentage photodegradation of methylene blue by Pt-N-TiO2 and Pt-N-TiO2/RHEAC. C0 and Cf are the initial and final methylene blue concentrations in the reaction mixture, respectively.

Table 3: L9 OA experimental design table with results and the corresponding S/N ratios

Exp. No.	Process parameters				% Photodegradation (η)		S/N ratios of results (dB)	
	C	*A*	*T*	*P*	η1	η2	η1	η2
1	15	0.3	60	5.5	49.56	60.18	33.90	35.59
2	15	0.6	90	7.0	73.36	79.96	37.31	38.06
3	15	0.9	120	8.5	93.11	98.92	39.38	39.91
4	25	0.3	90	8.5	52.55	59.57	34.41	35.50
5	25	0.6	120	5.5	72.32	82.72	37.19	38.35
6	25	0.9	60	7.0	85.42	92.78	38.63	39.35
7	35	0.3	120	7.0	39.78	51.12	31.99	34.17
8	35	0.6	60	8.5	49.00	63.68	33.80	36.08
9	35	0.9	90	5.5	80.22	84.52	38.09	38.54

Results and Discussion

Characterization

The BET surface area (SBET) of the as-prepared photocatalysts were measured by employing the N2 adsorption-desorption isotherms shown in Figure 1. as can be observed, the photocatalysts both exhibited the conventional type IV isotherm curve with an H1 type hysteresis loop following IUPAC classification, indicating capillary condensation in mesoporous structure with well-defined cylindrical pore channels. The Barrett-Joyner-Halenda (BJH) model was used to determine the pore size distribution of the photocatalysts from the desorption branch of the isotherms (inserts Figure 1a and 1b). The physicochemical characteristics of the photocatalysts such as SBET, total pore volume (Vp), and pore diameter (Pd) are presented in Table 4. The large surface area and porosity of Pt-N-TiO2/RHEAC photocatalyst compared to the surface area and porosity of Pt-N-TiO2 account for the higher photocatalytic efficiencies of Pt-N-TiO2/RHEAC compared to Pt-N-TiO2.

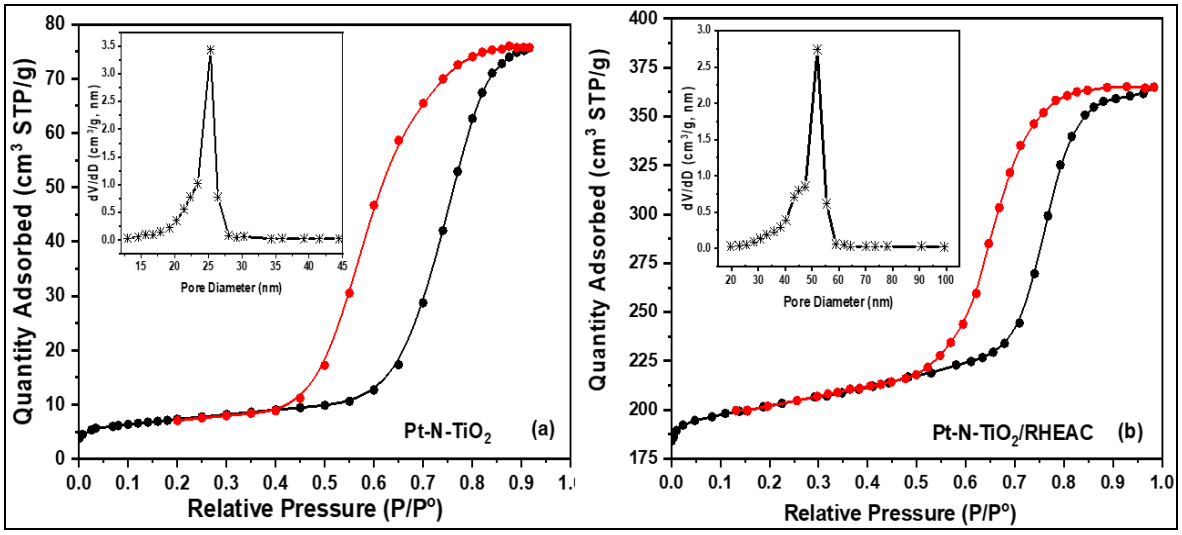

Fig 1: N2 adsorption-desorption isotherms of (a) Pt-N-TiO2 and (b) Pt-N-TiO2/RHEAC

Table 4: Physicochemical properties of the as-prepared photo catalysts.

Photocatalysts	Vm (cm3/g)	SBET (m2/g)	Pore Volume (cm3/g)	Pore diameter (nm)	Bandgap (eV)
Pt-N-TiO2	5.834	25.41	0.009	27.86	3.05
Pt-N-TiO2/RHEAC	152.6	664.7	0.236	37.09	2.83

The optical absorption spectra of the as-prepared photocatalysts Pt-N-TiO2 and Pt-N-TiO2/RHEAC were recorded at room temperature in the wavelength range of 200 to 800nm as depicted in Figure 2a. Both samples showed absorption in the UV region as can be observed from the figure. The optical bandgap energies of the prepared photocatalysts were obtained by using the Tauc plot method using equation (3) [35].

$$(\alpha h\nu)^{1/n} = B(h\nu - E_g) \quad (3)$$

where @ is the absorption coefficient, h is the Planck constant, ν is the photon's frequency, B is the energy-independent constant, Eg is the bandgap energy, and n depends on the nature of the electron transition and is equal to ½ for direct and 2 for indirect allowed transition.

A Tauc plot obtained by plotting (αhν) 2 against hν for direct bandgap energy is shown in Figure 2b. the bandgap energies of the photocatalysts were determined from the extrapolated tangents constructed from the linear portions of the curve to the hν axis to be 3.16eV, 3.05eV and 2.83eV for TiO2, Pt-N-TiO2 and Pt-N-TiO2/RHEAC respectively.

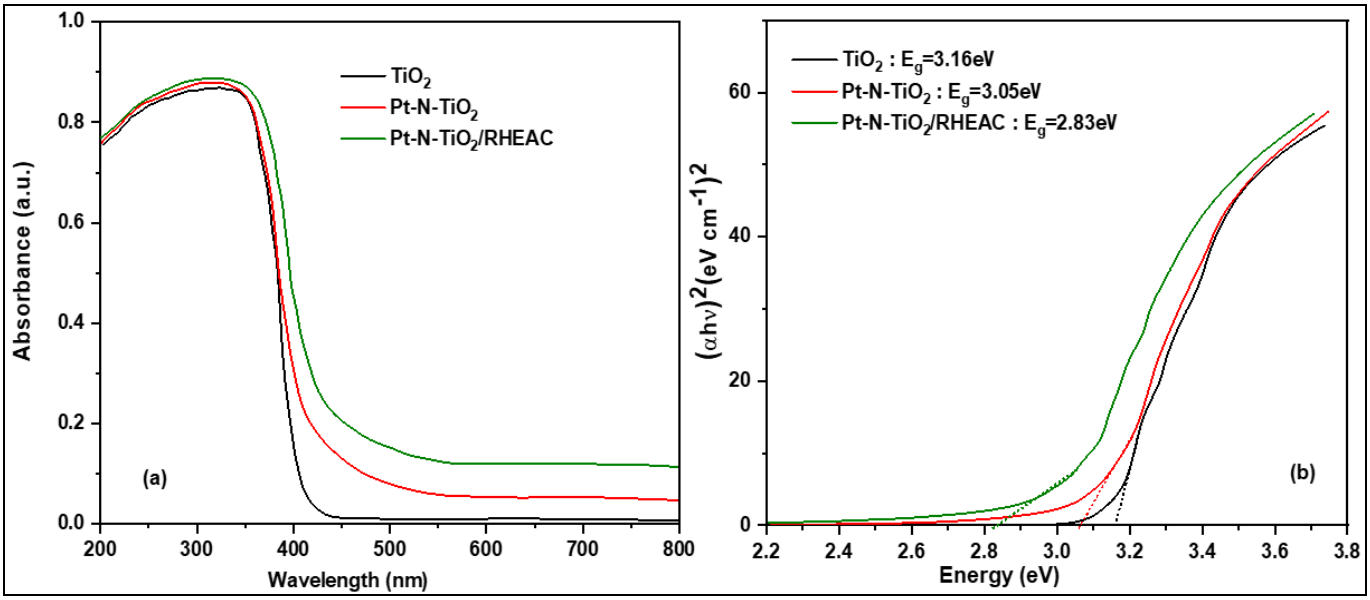

Fig 2: (a) UV-Vis diffuse absorption spectra of the as-prepared photocatalysts and (b) corresponding direct bandgap energies

UV-Vis absorption spectra of the photodegradation of MB by the as-prepared photocatalysts are presented in Figure 3. The spectra were recorded within a wavelength range of 400 to 800nm at different irradiation times. It can be noticed from the plots that maximum absorption occurred at a wavelength of 664nm for both photocatalysts. Likewise, it could be observed that the absorption peaks decreased with an increase in irradiation time due to the degradation of the chromophore responsible for the characteristic colour of MB with sustained UV irradiation.

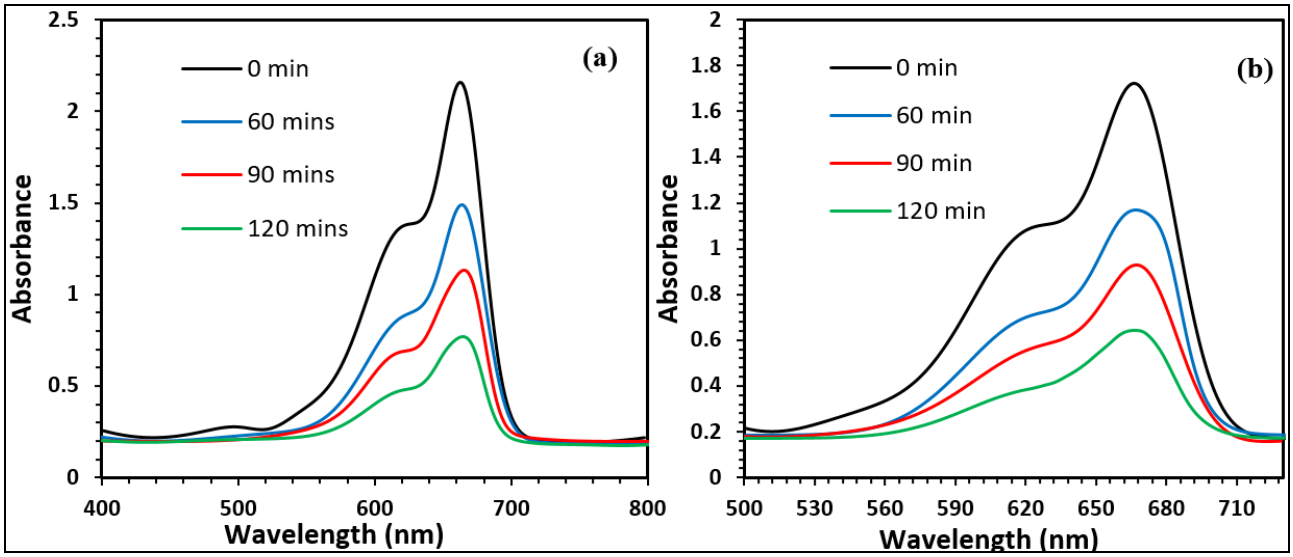

Fig 3: UV-Vis absorption spectral of MB solution catalyzed by (a) Pt-N-TiO2 and (b) Pt-N-TiO2/RHEAC

Statistical Optimization

Effect of process factors on η1 and η2

The direct effect of process factors on the response and dependent variables is known as the main effect. The main effects are plotted by taking into consideration the mean of response at each of the process factors. From Figures 4 and 5, which represent the main effects plot for the mean of response data, it can be observed that the photodegradation efficiency of MB by both Pt-N-TiO2 (η1) and Pt-N-TiO2/RHEAC (η2) diminished with an increase in dye concentration due to saturation of catalyst surface by MB molecules at high concentration and the absorption of UV light photons by some of the MB dye molecules [36, 37]. η1 and η2 increased with an increasing amount of catalyst as a result of the fact that increasing the catalyst amount results in an increase in the number of active sites available on the photocatalysts for the photodegradation process [38]. Similarly, Figures 4 and 5 revealed that η1 and η2 increased with an increase in irradiation time. Generally, photodegradation efficiency increase with irradiation time until the catalyst is consumed then the photodegradation efficiency starts decreasing [37]. photocatalytic degradation of dyes depends principally on pH due to its effect on the surface charge of the catalyst [37]. The efficiency of the photodegradation process is high in an acidic medium because positive holes which act as the principal oxidation species at low pH interact with hydroxide ions producing hydroxyl radicals which assist in the degradation process [39]. As illustrated in Figures 4 and 5, η1 and η2 decrease with an increase in pH.

In Tables 5 and 6, the column for rank reveals that the amount of catalyst ranked 1st contributes more to the photodegradation efficiencies of MB by both photocatalysts, this is followed by dye concentration ranked 2nd, then irradiation time ranked 3rd. pH contributes the least to η1 and η2.

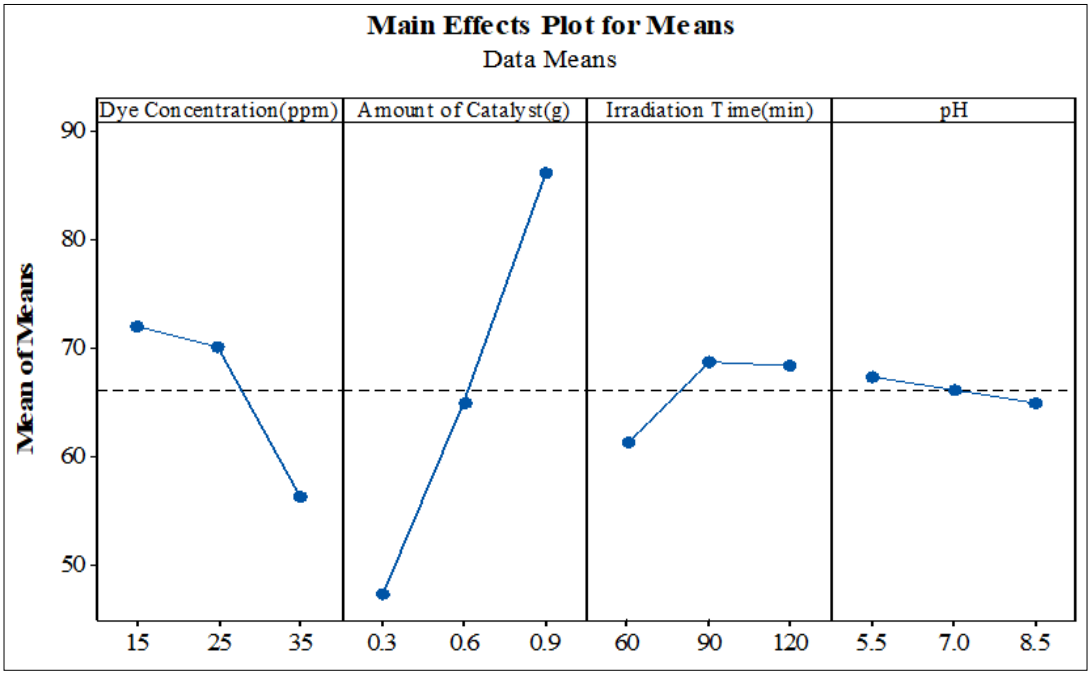

Fig 4: Main effects plot for Mean of Means for η1

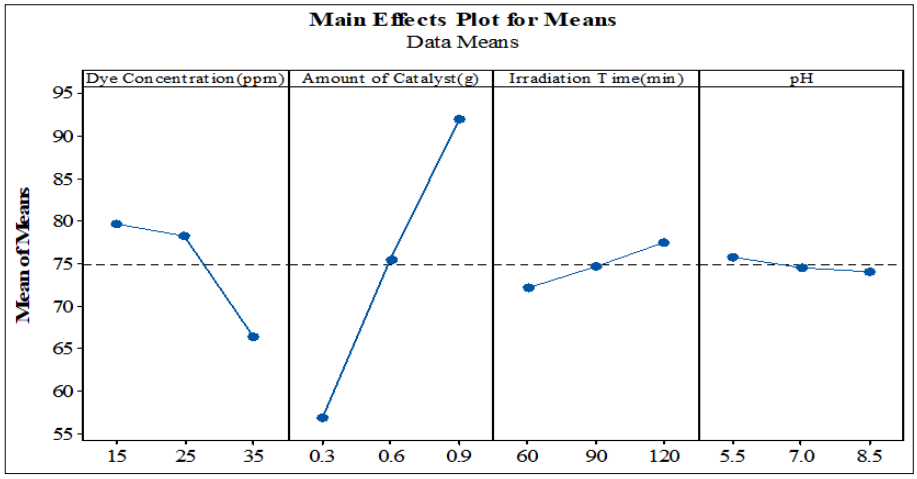

Fig 5: Main effects plot for Mean of Means for η2

Optimum Factor Levels Selection

The optimum level for a factor is the level that has the maximum S/N ratio. Higher S/N ratios indicate that there is a minimum variation difference between the targeted output and the measured output [40]. Figure 6 and 7 portrays the mean S/N ratio plots for methylene blue photodegradation efficiency for Pt-N-TiO2 (η1) and Pt-N-TiO2/RHEAC (η2), while Table 5 and 6 presents data on the mean S/N ratio response table for both η1 and η2. It can be inferred from both Tables 5 and 6 and from Figures 6 and 7 that, the optimum conditions of dye concentration, amount of catalyst, irradiation time, and pH for the photodegradation of methylene blue by both Pt-N-TiO2 and Pt-N-TiO2/RHEAC are *C1A3T2P1* and *C1A3T3P1* respectively. Consequently, it can be established that these optimum settings would give the highest S/N ratios and maximum photodegradation efficiency.

Table 5: Mean S/N ratio response table for η1

Process Parameter	Symbol	Mean S/N ratio					Optimum settings
		Level 1	Level 2	Level 3	Max. – Min.	Rank	
Dye Concentration	*C*	36.86	36.74	34.63	2.23	2	*C1*
Amount of Catalyst	*A*	33.44	36.10	38.70	5.26	1	*A3*
Irradiation Time	*T*	35.45	36.60	36.19	1.15	3	*T2*
pH	*P*	36.39	35.98	35.87	0.52	4	*P1*

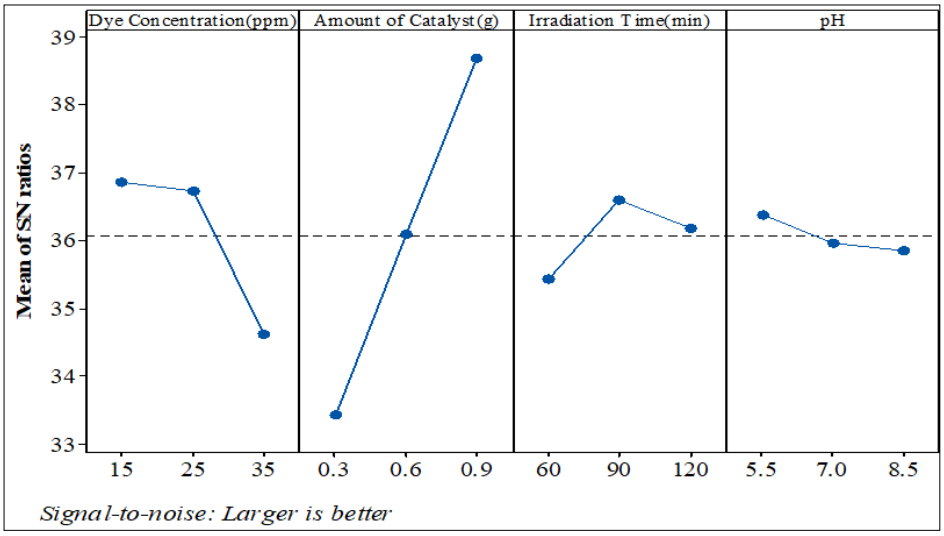

Fig 6: Main effect plot for Mean S/N ratio for η

Table 6: Mean S/N ratio response table for η2

Process Parameter	Symbol	Mean S/N ratio					Optimum settings
		Level 1	Level 2	Level 3	Max. – Min.	Rank	
Dye Concentration	*C*	37.85	37.73	36.26	1.59	2	*C1*
Amount of Catalyst	*A*	35.09	37.50	39.26	4.17	1	*A3*
Irradiation Time	*T*	37.01	37.37	37.48	0.47	3	*T3*
pH	*P*	37.49	37.19	37.16	0.33	4	*P1*

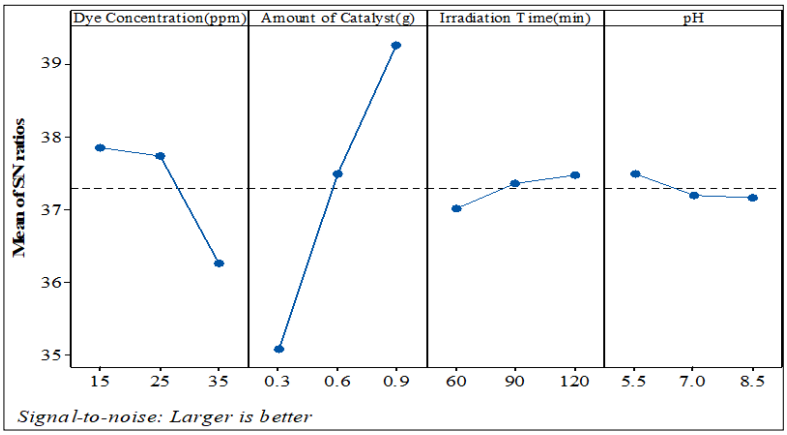

Fig 7: Main effect plot for Mean S/N ratio for η2

Modeling

In this work, linear regression analysis in Minitab version 17 was utilized in developing the additive models for the response variables η1 and η2 as a function of the process parameters. The addictive model equations gotten from the regression analysis are illustrated by equations 4 and 5.

$$\eta_1 = 42.0 - 0.784 * C + 64.92 * A + 0.1179 * T - 0.83 * P \qquad (R^2 = 96.23\%) \qquad (4)$$

$$\eta_2 = 52.3 - 0.662 * C + 58.53 * A + 0.0896 * T - 0.58 * P \qquad (R^2 = 97.38\%) \qquad (5)$$

The coefficient of determination (R2) was used to evaluate the adequacy of the developed mathematical models [41]. From the analysis, the coefficient of determination for the regression models which stood at 96.23% for η1 and 97.38% for η2 respectively were indicatory that the models could be utilized effectively in predicting the response variables at optimum factor levels.

The deviations of the data values obtained experimentally from the predicted values are represented in terms of residuals. Thus, the residual plot can be utilized to verify the significance of the coefficients in the regression models. If the normal probability plot of the residuals is a straight line, then the residual errors in the said models follow a normal distribution and the coefficients in the models are significant [42]. Figure 8 depicts the normal probability plot of residuals for η1 and η2. From the figure, it can be visualized that for both η1 and η2 the residuals are located about the straight line indicating the coefficients of the developed models are significant.

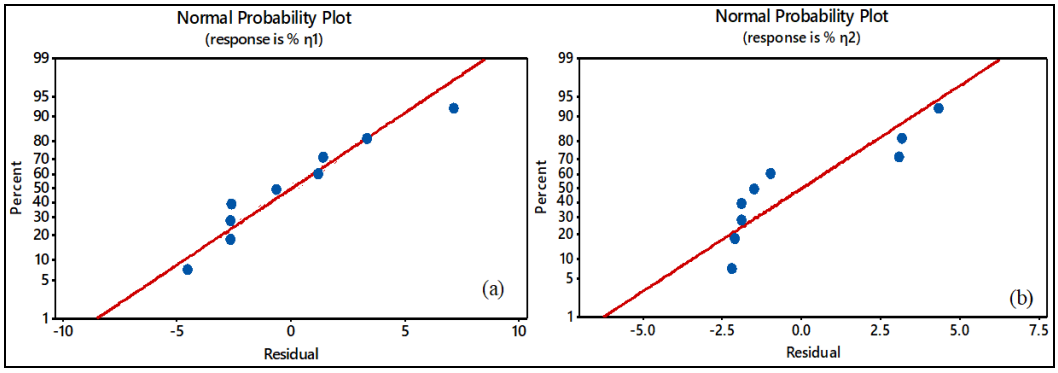

Fig 8: Normal probability plot of residuals for η1and η2

Analysis of Variance

Analysis of Variance (ANOVA) was conducted with the view to determining the process parameters that remarkably influence the response variable. Pooled error sum of squares procedure was applied and the ANOVA results for the percentage photodegradation of methylene blue by Pt-N-TiO2 and Pt-N-TiO2/RHEAC are presented in Table 7 and 8 respectively. The results of the ANOVA revealed that the amount of catalyst was the prime contributor to the photocatalytic degradation of methylene blue by both Pt-N-TiO2 and Pt-N-TiO2/RHEAC, with percentage contributions of 77.58% and 83.38% respectively. Dye concentration contributed 17.72% to the percentage photodegradation by Pt-N-TiO2 and 14.84% to the percentage photodegradation by Pt-N-TiO2/RHEAC. The above results agree with the process parameter ranking as exemplified in Tables 5 and 6. Also, it can be inferred from Tables 7 and 8 that irradiation time and pH with p-values of 0.302 and 0.718 for photodegradation by Pt-N-TiO2 and 0.370 and 0.545 for photodegradation by Pt-N-TiO2/RHEAC respectively which are all greater than 0.05 did not have statistical significance at 95% confidence level.

Table 7: ANOVA of % photodegradation for Pt-N-TiO2 (* Pooled factors)

Source	Degree of freedom	Sum of Squares	Mean Squares	F-ratio	P-value (p<0.05)	% Contribution
Dye Concentration(ppm)	2	9.4889	4.7444	7.54	0.045	17.72
Amount of Catalyst(g)	2	41.5529	20.7764	33.0	0.033	77.58
Irradiation Time(min)	2	2.0577*	1.0289	1.64	0.302	3.84

pH	2	0.4602*	0.2301	0.36	0.718	0.86
Pooled error	4	2.5179	0.6295			
Total	8	53.5597				100.00

Table 8: ANOVA of % photodegradation for Pt-N-TiO2/RHEAC (* Pooled factors)

Source	Degree of freedom	Sum of Squares	Mean Squares	F-ratio	P-value (p<0.05)	% Contribution
Dye Concentration(ppm)	2	4.6940	2.3470	16.63	0.012	14.84
Amount of Catalyst(g)	2	26.3831	13.1916	93.49	0.000	83.38
Irradiation Time(min)	2	0.3630*	0.1815	1.29	0.370	1.14
pH	2	0.2012*	0.1006	0.71	0.545	0.64
Pooled error	4	0.5642	0.1411			
Total	8	31.6413				100.00

Prediction of performance characteristics under optimum conditions

Once the optimal levels of the process factors have been ascertained, the next step is to predict and validate the quality characteristics (response variables or S/N ratio) by applying the optimal levels of the process factors using equation (6) [43].

$$\gamma_{predicted} = \gamma_m + \sum_{i=1}^{n}(\gamma_i - \gamma_m) \quad (6)$$

where γm is the total mean of the response variable or S/N ratio, γi is the mean of the optimal level of response variable or S/N ratio corresponding to ith significant factor on jth level, n is the number of significant factors.

Since the sum of squares of irradiation time and pH are very small and were utilized in the estimation of the error variance, these terms were not included in the calculation of the predicted photodegradation efficiencies and S/N ratios at optimal levels of the process factors for both photocatalysts.

Tables 9 and 10 presents the results of the confirmation experiments for η1 and η2 performed with the optimal levels of the process factors. From the tables, it could be observed that optimal parameters settings led to an improvement in the predicted photodegradation efficiency and S/N ratio for the photodegradation of MB by both catalysts, as compared to the initial process parameter settings.

Confirmation experiments at optimal levels of process parameters revealed a 30.15% and 25.07% increase in photodegradation efficiency (η) for both catalysts compared to the initial process parameters settings. Also, the confirmation experiments showed that the S/N ratios witnessed an improvement of 3.118 dB for η1 and 2.501 dB for η2 at optimal levels of process parameters compared to the initial process parameters settings. It is thus evident that optimal process parameters settings led to higher photodegradation efficiencies and S/N ratios for both photocatalysts.

Table 9: Confirmation results for η and S/N ratio by Pt-N-TiO2

	Initial process parameter	Optimal process parameters	
		Predicted	Experimental
Level	*C2-A2-T2-P2*	*C1-A3-T2-P1*	*C1-A3-T2-P1*
% photodegradation (η)	66.153	92.110	94.714
Percentage increase (η)	30.15 %		
S/N ratio (dB)	36.410	40.322	39.528
Improvement in S/N ratio (dB)	3.118		

Table 10: Confirmation results for η and S/N ratio by Pt-N-TiO2/RHEAC

	Initial process parameter	Optimal process parameters	
		Predicted	Experimental
Level	*C2-A2-T2-P2*	*C1-A3-T3-P1*	*C1-A3-T3-P1*
% photodegradation (η)	74.872	96.930	99.921
Percentage increase (η)	25.07 %		
S/N ratio (dB)	37.486	40.237	39.993
Improvement in S/N ratio (dB)	2.507		

Confirmation results analysis for the developed models

Analysis of experimental results was performed to validate the developed regression models. Odd-numbered experiments were considered from the L9 orthogonal array experimental design for the analysis and the results are presented in Table 11. It can be inferred from the results of the analysis that a substantive reasonable agreement exists between the experimental results and the predicted photodegradation efficiencies obtained by employing the model equations for both photocatalysts.

Table 11: confirmation results for the developed regression models

Exp. No.	Experimental		Predicted		Residual		% Error	
	η1	η2	η1	η2	η1	η2	η1	η2
1	49.56	60.18	52.21	62.12	-2.65	-1.94	5.35	3.22
3	93.11	98.92	95.76	100.87	-2.65	-1.95	2.85	1.97
5	72.32	82.72	70.94	78.43	1.38	4.29	1.91	5.19
7	39.78	51.12	42.37	53.38	-2.59	-2.26	6.51	4.42
9	80.22	84.52	79.03	86.68	1.19	-2.16	1.48	2.56

Conclusion

The photocatalytic degradation of methylene blue dye in an aqueous solution was investigated in this study, using the Taguchi design with importance given to process parameters such as dye concentration, amount of catalyst, irradiation time, and pH. Both photocatalysts (Pt-N-TiO2 and Pt-N-TiO2/RHEAC) synthesized by the sol-gel method exhibited a mesoporous structure with bandgap energies of 3.05eV and 2.83eV and particle sizes of 27.86nm and 37.09nm respectively.

The optimal conditions to obtain maximum photodegradation of MB were as follows: dye concentration=15ppm, amount of catalyst=0.9g, irradiation time=90min, and pH=5.5 for Pt-N-TiO2 photocatalyst while for Pt-N-TiO2 photocatalyst there were: dye concentration=15ppm, amount of catalyst=0.9g, irradiation time=120min, and pH=5.5. Under these optimal conditions, the photodegradation efficiency was 94.71% for Pt-N-TiO2 and 99.92% for Pt-N-TiO2/RHEAC.

From the ANOVA for both photocatalysts, the amount of catalyst was observed to be the principal contributor to the photodegradation efficiency, contributing 77.58% and 83.38% to the photodegradation efficiencies by Pt-N-TiO2 and Pt-N-TiO2/RHEAC respectively. This was followed by dye concentration. Irradiation time and pH were statistically insignificant.

From a view of the developed mathematical models for η1 and η2, a reasonable agreement was observed between the predicted and the experimental response characteristics. Also, the coefficients of determination (R2) of 96.23% for η1 and 97.38% for η2 were indicatory that the models could be employed effectively in predicting the response characteristics at optimum process parameters level.

References

1. Aguila DMM, Ligaray MV. Adsorption of Eriochrome Black T on MnO2-coated zeolite. International Journal of Environmental Science and Development,2015:6(11):824-827.
2. Kazemi F, Mohamadnia Z, Kaboudin B, Karimi Z. Photodegradati1on of methylene blue with a titanium dioxide/polyacrylamide photocatalyst under sunlight. Journal of Applied Polymer Science,2016:133:43386:1-9.
3. Hou C, Hu B, Zhu Z. Photocatalytic degradation of methylene blue over TiO2 pretreated with varying concentrations of NaOH. *Catalysts*,2018:8(575):1-13.
4. Lu C, Sun X, Peng J, Ma Y. The preparation of ternary nanocomposite TiO2/ZrO2/SnO2 by double template and application for water purification. J. of Chem. Soc. Pak,2013:35(1):42-48.
5. Joseph N, Vellayan K, González B, Vicente MA, Gil A. Effective degradation of methylene blue in aqueous solution using Pd supported Cu-doped Ti-pillared montmorillonite catalyst. *Appl. Clay Sci*,2019:168:7-10.
6. Samsudin MF, Sufian S, Bashiri R, Mohamed NM, Siang LT, Ramli RM. Optimization of photodegradation of methylene blue over modified TiO2/BiVO4 photocatalysts: Effects of total TiO2 loading and different type of co-catalyst. *Mater. Today Proc*,2018:5:21710-21717.
7. Khaksar M, Amini M, Boghaei DM, Chae KH, Gautam S. Mn-doped ZrO2 nanoparticles as an efficient catalyst for green oxidative degradation of methylene blue. *Catal. Commun*,2015:72:1-5.
8. Kong L. Diao Z, Chang X, Chen D. Synthesis of recoverable and reusable granular MgO-SCCA-Zn hybrid ozonation catalyst for degradation of methylene blue. J. Environ. Chem,2016:4:4385-4391.
9. Abbas M, Rao BP, Reddy V, Kim C. Fe3O4/TiO2 core/shell nanocubes: Single-batch surfactantless synthesis, characterization and efficient catalysts for methylene blue degradation. *Ceram. Int*,2014: 40:11177-11186.
10. Mishra DD, Tan G. Visible photocatalytic degradation of methylene blue on magnetic SrFe12O19. J. Phys. Chem. Solids,2018:123:157-161.
11. Adeleke JT, Theivasanthi T, Thiruppathi M, Swaminathan M, Akomolafe T, Alabi AB. Photocatalytic degradation of methylene blue by ZnO/NiFe2O4 nanoparticles. *Appl. Surf. Sci*,2018:455:195-200.
12. Huang D, Ma J, Fan C, Wang K, Zhao W, Peng M, *et al*. Co-Mn-Fe complex oxide catalysts from layered double hydroxides for decomposition of methylene blue: Role of Mn. *Appl. Clay Sci*,2018:152:230-238.
13. Ganesh RS, Durgadevi E, Navaneethan M, Sharma SK, Binitha HS, Ponnusamy S, *et al*. Visible light induced photocatalytic degradation of methylene blue and rhodamine B from the catalyst of CdS nanowire. *Chem. Phys. Lett*,2017:684:126-134.
14. Liao G, Li Q, Zhao W, Pang Q, Gao H, Xu Z. In-situ construction of novel silver nanoparticle decorated polymeric spheres as highly active and stable catalysts for reduction of methylene blue dye. *Appl. Catal. A Gen*,2018:549:102-111.
15. Veziroglu S, Kuru M, Ghori MZ, Dokan FK, Hinz AM, Strunskus T, *et al*. Ultra-fast degradation of methylene blue by Au/ZnO-CeO2 nano-hybrid catalyst. *Mater. Lett*,2017:209:486-491.
16. Darzi SJ, Mahjoub AR, Sarfi F. Visible light active nitrogen doped TiO2 nanoparticles prepared by sol-gel acid catalyzed reactions. Iranian Journal of Material Science and Engineering,2012:9(3):17-23.
17. Wang XJ, Song JK, Huang JY, Zhang J, Wang X, Ma RR, *et al*. AC-based magnetic TiO2 photocatalyst co-doped with iodine and nitrogen for organic pollution degradation. Appl. Surf. Sci,2016:390:190-201.
18. Le SK, Jiang TS, Li YW, Zhao Q, Li YY, *et al*. Highly efficient visible-light-driven mesoporous graphitic carbon nitride/ZnO nanocomposite photocatalysts. *Appl. Catal. B Environ*,2017:200:601-610.
19. Busko TO, Kulish MP, Dmytrenko OP, Vityuk NV, Eremenko AM. Electron structure of TiO2 composite films with noble metal nanoparticles. *Semiconductor Physics, quantum Electronics and Optoelectronics*,2014:17(1):67-74.
20. Bhirud A, Sathaye S, Waichal R, Park CJ, Kale B. In situ preparation of N-ZnO/grapheme nanocomposites: Excellent candidate as a photocatalyst for enhanced solar hydrogen generation and high-performance supercapacitor electrode. J. Mater. Chem. A,2015:3:17050-17063.
21. Jaramillo-Páez C, Navío JA, Hidalgo MC, Macías M. High UV-photocatalytic activity of ZnO and Ag/ZnO synthesized by a facile method. *Catal. Today*,2017:284:121-128.
22. Hashimoto K, Irie H, Fujishima A. TiO2 photocatalyst:

A historical overview and future prospects. Japanese Journal of Applied Physics,2005:44(12):8269-8285.
23. Jang YJ, Jang YH, Kim DH. Nanostructuredcarbon-TiO2 shells onto silica beads as a promising candidate for the alternative photoanode in dye-sensitized solar cells. *Sci. Adv. Mater*,2015:7:956-963.
24. Vaiano V, Sacco O, Sannino D, Ciambelli P. Nanostructured N-doped TiO2 coated on glass spheres for the photocatalytic removal of organic dyes under UV or visible light irradiation. *Appl. Catal. B Environ*,2015:*170:*153-161.
25. Vandana Sukhadia. Photo catalytic degradation of copper surfactant. Int. J Adv. Chem. Res. 2020;2(2):53-55. DOI: 10.33545/26646781.2020.v2.i2a.63
26. Gar Alalm M, Tawfik A, Ookawara S. Solar photocatalytic degradation of phenol by TiO2/AC prepared by temperature impregnation method. *Desalination Water Treat*,2014:*57:*835-844.
27. Ragupathy S, Raghu K, Prabu P. Synthesis and characterization of TiO2 loaded cashew nut shell activated carbon and photocatalytic activity on BG and MB dyes under sunlight radiation. *Spectrochim. Acta A*,2015:138:314-320.
28. Liu DD, Wu ZS, Tian F, Ye BC, Tong YB. Synthesis of N and La co-doped TiO2/AC photocatalyst by microwave irradiation for the photocatalytic degradation of naphthalene. J. Alloys Compd,2016:676:489-498.
29. Okcu GD, Tunacan T, Dikmen E. Removal of indigo dye by photocatalysis process using Taguchi experimental design. *Enviromental Research and Technology*,2019:2(2):63-72.
30. Daneshvar N, Khataee AR, Rasoulifard MH, Pourhassan M. Biodegradation of dye solution containing Malachite Green: Optimization of effective parameters using Taguchi method. Journal of Hazardous Materials,2007:143(1-2):214-219.
31. Hiragond CB, Kshirsagar AS, Khanna DP, More PVM, Khanna PK. Electro-photocatalytic degradation of methylene blue dye using various nanoparticles: A demonstration for undergraduates. Journal of Nanomedicine Research,2018:7(4):254-257. DOI:10.15406/jnmr.2018.07.00195
32. Moradi R, Hamidvand M, Ganjali A. Using of TiO2/Ag2O Nanocomposite in Degradation of Acid Red 18 Dye in Photoreactor by Taguchi Experimental Design. Russian Journal of Physical Chemistry A,2019:93(6):1133-1142.
33. Roy RK, A primer on the Taguchi method, 2nd edition. Society Manufacturing Engineers, New York, 2010.
34. Chen X, WuZ, Gao Z, Ye BC. Effect of Different Activated Carbon as Carrier on the Photocatalytic Activity of Ag-N-ZnO Photocatalyst for Methyl Orange Degradation under Visible Light Irradiation. *Nanomaterials*,2017:7(258):1-1.
35. Makula P, Pacia M, Macyk W. How to correctly determine the band gap energies of modified semiconductor photocatalysts base on UV-Vis spectra. Journal of Physical Chemistry Letters,2018:9:6814-6817.
36. Yao J, Wang C. Decolorization of methylene Blue with TiO2 sol via UV irradiation photocatalytic degradation. International Journal of Photoenergy, 2010, 1-6.
37. Salama A, Mohamed A, Aboaera NM, Osman OTA, Khattah A. Photocatalytic degradation of organic dyes using composite nanofibers under UV irradiation. Applied Nanoscience,2018:8:155-161.
38. Shojaei S, Shojaei S. Experimental design and modelling of removal of acid green 25 dye by nanoscale zero-valent iron. Euro-Mediterr. J. Environ. Integr., 2017, 2-15.
39. Marandi R, Sharif AAM, Olya ME. Preparation, characterization of NiFe2O4 nanoparticles supported on Clinoptilolite and optimization of photocatalytic degradation of pollutants in textile wastewater by Taguchi experimental design. Journal of Basic and Applied Scientific Research,2013:3(8):443-456.
40. Sivaiah P, Chakradhar D. Modeling and optimization of sustainable manufacturing ptocess in machining of 17-4PH stainless steel. Measurement, 2018. doi: https://doi.org/10.1016/j.measurement.2018.10.06.
41. Muluh NK, Ghogomu JN, Tamungang NEB. application of the box-behnken design for modelling and optimization of direct red 81 adsorption usig raffia palm (Raphia Hookeri) fruit epicarp activated carbon. International Journal of Research in Advanced Engineering and Technology,2017:2(3):15-24.
42. Panda AK, Singh RK. Optimization of process parameters by Taguchi method: Catalytic degradation of polypropylene to liquid fuel. International Journal of Multidisciplinary and Current Research. July-August, 2013, 50-58.
43. Haq AN, Marimuthu P, Jeyapaul R. Multi response optimization of machining parameters of drilling Al/SiC metal matrix composite using grey relational analysis in the Taguchi method. Int J Adv Manuf Technol.,2008:37:250-255.
44. Wang JJ, Jing YH, Ouyang T, Chang CT. Preparation of 13X from waste quartz and photocatalytic reaction of methyl orange on TiO2/ZSM-5, 13X and Y-zeolite. J. Nanosci. Nanotechnol,2015:15:6141-6149.